Received: 13 June 2024 | Revised: 4 May 2025 | Accepted: 8 May 2025

DOI: 10.1002/esp.70086

RESEARCH ARTICLE

ESPL WILEY

The impact of outer-bar alongshore variability on inner-bar rip dynamics

Drude Fritzbøger Christensen[1,2] | Britt Raubenheimer[2] | Steve Elgar[2]

[1]Department of Geosciences and Natural Resource Management, University of Copenhagen, Copenhagen K, Denmark

[2]AOPE Department, Woods Hole Oceanographic Institution, Woods Hole, MA, USA

Correspondence
Drude Fritzbøger Christensen, Department of Geosciences and Natural Resource Management, University of Copenhagen, Øster Voldgade 10, 1350 Copenhagen K, Denmark.
Email: dc@ign.ku.dk

Funding information
Vannevar Bush Faculty Fellowship; Villum Fonden, Grant/Award Number: 37163; US National Science Foundation

Abstract

A field-calibrated morphodynamic model (MIKE21) is used to investigate the importance of the dimensions of a rip channel across an outer sand bar to the hydrodynamics and morphological evolution of an inner sand bar and rip channel for a range of initial bathymetries and wave conditions. The model was driven with offshore wave conditions and idealized bathymetry representative of field conditions near Duck, NC, USA during which strong rips and associated channel erosion were observed to occur over an inner bar. Consistent with prior results, the strength of the hydro-morphological coupling between the two bars depends on the dimensions of the outer-bar perturbation, as well as the wave forcing. The results suggest that in double-barred systems, a single moderate-scale perturbation (O(0.1 m deep, 10 m wide)) in the outer-bar elevation can lead to the generation of a rip current and associated erosion of a rip channel across the inner bar. The simulations suggest that the magnitude of the inner-bar rip flow, the depth to which the inner-bar channel is eroded, and the alongshore position of the inner-bar rip relative to the outer-bar perturbation depend on the non-dimensional outer-bar channel depth, the transverse rip-channel slope, and the wave height, period and directional spreading. For deep and narrow outer-bar channels, the outer-inner bar coupling is strong. In contrast, for shallow and wide outer-bar channels, the system may alternate between being coupled and uncoupled with unstable locations of the inner-bar rip.

KEYWORDS
coastal erosion, double-bar systems, numerical modelling, rip channels, surfzone

1 | INTRODUCTION

Double sand bar systems are observed worldwide on wave-dominated beaches (Almar et al., 2010; Anderson et al., 2023; Birkemeier, 1985; Ruessink et al., 2000; Splinter et al., 2018). The number of bars usually correlates with the nearshore slope, with only one sand bar on steep, reflective beaches (Evans, 1940), but the number is also dependent on wave conditions (Short & Aagaard, 1993). Similar to single bar systems, the bars can vary from shore-parallel linear bars to alongshore variable crescentic bars, sometimes intersected by "rip" channels (Short & Aagaard, 1993). Strong, offshore-directed flows often occur in the cross-shore oriented rip channels intersecting single or multiple bars. These rip currents are driven by converging alongshore-directed feeder currents forced by alongshore variable wave heights and directions (Dalrymple et al., 2011; Haller, Dalrymple, & Svendsen, 2002). Rip current strengths are of order 0.5 m/s (Houser et al., 2020) and therefore they are both a major risk to beachgoers (Brander, 2015; Dusek & Seim, 2013), and also of great importance for offshore sediment transport across the surf zone (Aagaard, Greenwood, & Nielsen, 1997) and beach erosion (Castelle, Marieu, & Bujan, 2019).

The hydrodynamics and morphology interact with the sand bar, affecting wave transformation and the generation of nearshore currents, which affect the exchange of sediment across the surf zone (Hoefel & Elgar, 2003; Lippmann, Holman, & Hathaway, 1993). Moreover, morphodynamics of the inner bar are affected by the wave transformation over the outer bar (e.g., wave breaking) (Klein &

Schuttelaars, 2006; Ruessink, Pape, & Turner, 2009), and the cross-shore distance between the bars is important for the morphological evolution of the double bar system (Coco et al., 2020; Ruessink et al., 2007). The length scale of the bar crescents or alongshore separation between rip channels can deviate between the inner and outer sand bars (Smit et al., 2008), and the bars may respond at different rates to changing wave conditions (Van Enckevort et al., 2004).

Field observations have indicated there may be morphological coupling between the inner and outer bar in a double bar system (Castelle et al., 2015; Price & Ruessink, 2011; Quartel, 2009; Ruessink et al., 2007) despite alongshore variability occurring at a narrower range of wavelengths in outer bars compared with that for inner bars (Van Enckevort et al., 2004). A combination of self-organization modeling and coupling between morphology, waves and flows onshore of a crescentic outer bar (wavelengths of 200–700 m and vertical amplitudes of 0.2–2.7 m) resulted in inner-bar rip channels of variable length-scales compared with the outer bar (Castelle et al., 2010a, 2010b). In this and other cases (Loureiro, Ferreira, & Cooper, 2012; Thornton, MacMahan, & Sallenger, 2007), the shoreline undulated with cusps and increased dune erosion onshore of bar crescents where rip currents concentrate.

Here, medium-scale perturbations (O(0.2 m depth, 75 m width)) were observed in an outer bar on a sandy beach near Duck, NC, USA (Figure 1) at the same alongshore positions as inner-bar channels and dune erosional hotspots (Elgar et al., 2023). The double-barred sandy beach near Duck was almost alongshore uniform in September 2013 before a moderate-high energy event passed between Sep. 25 and Oct. 2, 2013. After this event of near-normally incident waves with offshore significant wave heights (H_s) of approximately 2 m and peak wave periods (T_p) of 6 s, the inner bar bathymetry became highly alongshore variable with roughly 1-m-deep, 100-m-wide beach and dune erosional hotspots (Elgar et al., 2023, Figure 2b). The perturbations observed in the outer bar were smaller than those considered in prior studies of morphological coupling in double-bar systems. Hence, it is unknown whether the observed medium-scale perturbations were responsible for the evolution of inner-bar channels and dune erosional hotspots. The field observations thus motivated the aim of this study, which is to examine the importance of the depth and width of a single perturbation in an outer bar to rip generation across the inner bar.

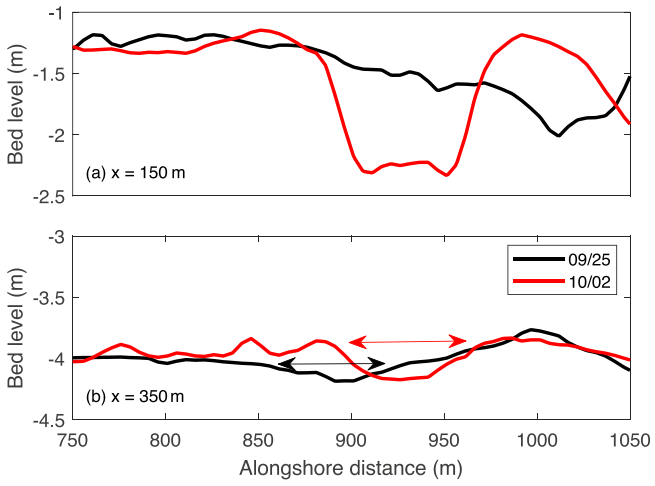

FIGURE 1 Bed level versus alongshore distance at (a) inner (cross-shore distance x = 150 m) and (b) outer (x = 350 m) bar crest positions on Sep. 25 (black curves) and Oct. 2 (red curves), 2013 near Duck, NC, USA. Black (red) arrow in (b) highlights a perturbation in the outer bar on Sep. 25 (Oct. 2).

Even though the evolution of crescentic bars and rip channels has been studied for decades (Bowen & Inman, 1969, 1971), this may be the first time a numerical morphodynamic model is used to explore the necessary dimensions of a single perturbation in an outer bar to affect an inner bar and to generate rip channels. Previous model explorations of rip channel evolution and coupling between bars are limited to self-organization models (Nnafie et al., 2021; Smit et al., 2008; Thiébot et al., 2012), where initial small-scale random perturbations (few centimetres) result in the formation of large-scale periodic morphological features or to the application of fully developed bathymetric templates of much larger scale alongshore variability (hundreds of meters) in the outer-bar (Castelle et al., 2010a, 2010b). In addition, while the applied morphodynamic model MIKE21 FM has been used widely to study hydrodynamics over complex bathymetry, only a few studies have used it to study couplings between hydrodynamics and morphological evolution (Badru et al., 2022; Cáceres, Zyserman, & Perillo, 2016; Petropoulos et al., 2022; Valipour & Bidokhti, 2018; Valipour, Khaniki, & Bidokhti, 2014). Recently, MIKE21 was used to model observed trends in flow and bathymetric evolution for two dredged (rip) channels across an inner sandbar in fall 2012 on the same sandy beach near Duck, NC, USA where the double-barred system was observed in 2013 (Christensen, Raubenheimer, & Elgar, 2024b; Moulton et al., 2017). The model calibrations from that study are re-applied on medium-scale bathymetric templates (tens of meters) to study the necessary outer-bar perturbation dimensions for bar coupling to arise and for nearshore rip channels to erode.

2 | METHODS

2.1 | Model set-up and initial bathymetries

The phase- and depth-averaged numerical model MIKE21 FM (2017a; 2017b; DHI, 2020) is used to simulate flow and bathymetric feedbacks in a double-bar system. Based on the wave action conservation equation, Reynolds averaged Navier–Stokes equations, a sediment transport look-up table and the sediment continuity equation, the model simulates wave transformation, wave-induced currents, sediment transport and their interactions.

The sediment transport look-up table was generated using a sediment grain size of 0.2 mm with a grading coefficient of 1.51 and porosity of 0.4, consistent with conditions at Duck, NC (Gallagher, Elgar, & Guza, 1998). In addition, the bed concentration is estimated using a deterministic formula (Engelund & Fredsøe, 1976), applying a critical Shield's parameter of 0.05 and estimation of near-bed wave orbital velocities by use of a semi-empirical, non-linear model (Isobe & Horikawa, 1982). The sediment transport is calculated as the sum of bed load (Engelund & Fredsøe, 1976) and suspended load (Fredsøe, Andersen, & Silberg, 1985), and zero sediment flux gradients are applied along the open model boundaries.

Simulations are conducted on a flexible mesh extending 6,200 m alongshore and 1,000 m cross-shore, resulting in a total of 70,398

cells. The cell sizes vary between a maximum length of 8 m in the centre of the domain (alongshore coordinate 1,000–2,200 m and cross-shore coordinate 60–800 m) to 144 m along the domain boundaries. The mesh was extended alongshore outside the area of interest to avoid shadow zones from the obliquely incident waves that were applied only along the offshore boundary.

Simulations were run for 60 1,800-s time steps with a morphological speed-up factor of 4 so that the simulation outputs correspond to the bathymetric evolution over 120 hours or 5 days. To explore the observed system behaviour in 2013, simulations were run with wave conditions and duration mimicking the observed conditions during the moderate-high energy event at Duck in the fall of 2013. Hence, constant wave conditions of shore-normal waves with significant offshore wave heights of $H_s = 2$ m, a directional wave spreading (DSD) of 30°, wave periods of $T_p = 6$ s and a time-varying mean water level with an amplitude of ~0.6 m were applied to different initial bathymetries to study the effect of outer bar morphology on inner bar dynamics.

The model was run for two different double sand bar geometries representing an offshore (Case 1) and onshore (Case 2) migrating double bar system at Duck (Figure 2). The simulated profiles are based on values of bar top distance to the shore (Anderson et al., 2023, Figure 3e,f) and bar magnitudes (Anderson et al., 2023, Figure 3h,i) derived from a 41-year record of monthly surveyed cross-shore profiles at Duck, NC. The two typical sand bar states are associated with energetic (offshore migration) and calm (onshore migration) wave conditions, respectively. The sand bar geometries were chosen to mimic natural coastal morphology and cover morphological variability due to wave conditions.

The profiles were linearly interpolated to the model grid, and a perturbation was applied on the outer-bar crest in the centre of the domain (alongshore coordinate 1,600 m). Twenty-three cases were simulated with Gaussian-shaped perturbations in the range 0.16–0.68 m in the vertical and 24–77 m in the alongshore (Supporting information Table S1).

To explore further the influence of wave conditions on double-bar system hydrodynamics, 11 additional simulations were conducted for one bathymetric case (Case 2: 0.41 m deep and 49 m wide perturbation) without morphological updating. Wave conditions were within the range $H_s = 2$–6 m, $T_p = 6$–15 s and $DSD = 10$–30°. Furthermore, to support the morphodynamic findings based on the moderate-high energy event in 2013, simulations also were conducted for stronger forcing conditions ($H_s = 4$ m, $T_p = 10$ s and $DSD = 20°$) for a subset of the perturbation cases (Supporting Information Table S1, case numbers 5–6,8,13-14,17,21 and 23).

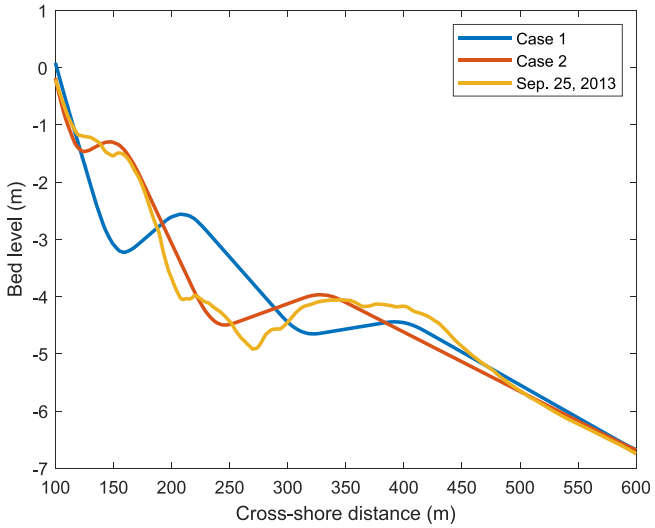

FIGURE 2 Bed level profiles versus cross-shore distance for offshore (blue curve) and onshore (red curve) migrating double bars at Duck based on Anderson et al. (2023), and for the surveyed profile at Duck on Sep. 25, 2013 (yellow curve).

2.2 | Rip current velocities and channel dimensions

Characteristic inner-bar rip current velocities are defined as the maximum offshore-directed flow within regions (Christensen, Raubenheimer, & Elgar, 2024b; Moulton et al., 2017). For hour 1, the region was defined as centered on the outer-bar alongshore channel

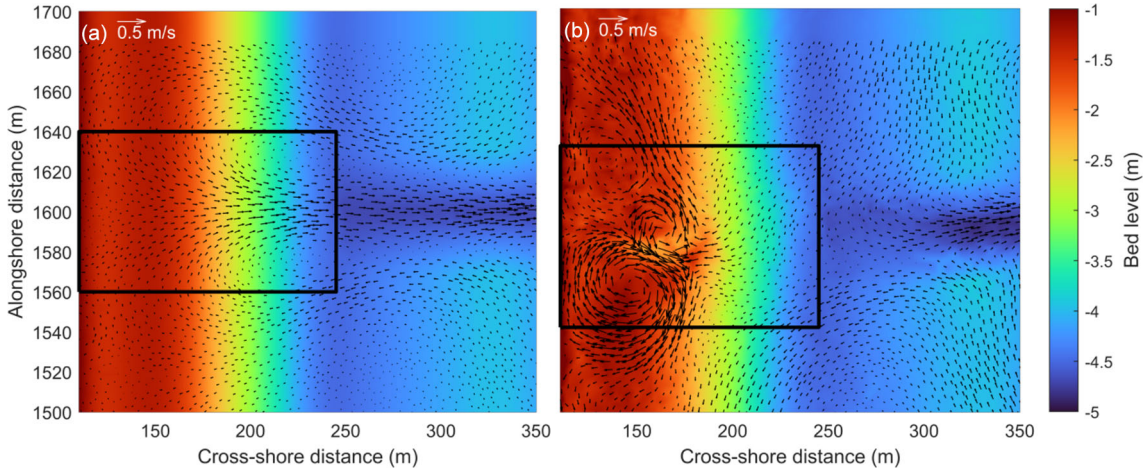

FIGURE 3 Examples of the flow patterns (arrows point in direction of flow with length proportional to speed, scale in upper left corners) for a case 2 simulation as a function of alongshore and cross-shore distance overlaid on color contours of the bathymetry (scale on the right) during hour (a) 1 and (b) 120. The inner-bar generated rip is visible in the black rectangles. The plots show only a central subset of the entire model domain.

coordinate (y = 1,600 m) ± 40 m, and from cross-shore coordinate x = 110 m to the outer-bar trough position, i.e., x = 320 m for the Case 1 bathymetry and x = 245 m for the Case 2 bathymetry (Figure 3a). For hour 120, the alongshore extent of the regions correspond to the positions of the eroded inner-bar channel sides ± 20 m (Figure 3b), where the channel sides are defined along the inner-bar crest (x = 210 m for Case 1 and x = 150 m for Case 2) as the positions where the bed level increase away from the channel center is less than 0.005 m (i.e., the minimum detected bed level change).

Rip current velocities depend on the water level (with stronger flows during low tide), and thus comparisons of flow velocities for different bathymetries (hour 1 versus hour 120) are only possible for similar water levels. Hydrodynamics were therefore simulated with a constant mean water level for both the initial (hour 1) and final (hour 120) bathymetry.

2.3 | Rip current forcings

The inner-bar rip currents are driven by the outer bar perturbations, which cause alongshore variable shallower-water waves that drive converging alongshore-directed feeder currents with magnitudes proportional to the bed stress given by (Haller, Dalrymple, & Svendsen, 2002; Kumar, Voulgaris, & Warner, 2011):

$$\text{alongshore bottom stress} = gh\frac{\partial \eta}{\partial y} + \frac{\partial S_{yy}}{\partial y} + \frac{\partial S_{xy}}{\partial x} + hU\frac{\partial V}{\partial x} + hV\frac{\partial V}{\partial y} \quad (1)$$

where g is gravitational acceleration, h is the total water depth, η is the wave-driven setup, S_{yy} and S_{xy} are the alongshore and diagonal components of the radiation stress, U and V are the mean cross- and alongshore velocities, and x and y are the cross- and alongshore coordinates. All terms are in units m^2/s^2 (i.e., radiation stresses are defined without including water density).

To compare the contributions to alongshore feeder flow convergence (which drives the rip current) between different simulation cases, the alongshore gradients in the bottom stress term are calculated at each cross-shore position from the outer-bar trough to the inner-bar crest during the first hour of the simulations. Specifically, at every cross-shore position between the outer-bar trough and inner-bar crest (Figure 4d, grey shaded area), the total of the alongshore stress terms (Equation 1) is calculated at each alongshore location (Figure 4a). The maximum southward (positive) and northward (negative) convergent stresses (black diamonds, Figure 4a) within the channel area (dotted lines in Figure 4a, e) are identified, and the stress gradient (∂(stress)/∂y) is calculated (Figure 4b, red dot being the result of Figure 4a).

The non-dimensional channel depth ($D = D_c/D_s$ where D_c is the maximum depth of the channel below the channel sides of depth D_s) and transverse slope ($SL = 2D_c/W$ where W is the channel width) of the outer bar perturbation control the alongshore setup gradients and wave refraction that are important drivers of rip currents (Moulton et al., 2017; Winter et al., 2014). These terms are combined into a nondimensional "DSL" parameter based on the initial bathymetries (hour 1) defined as:

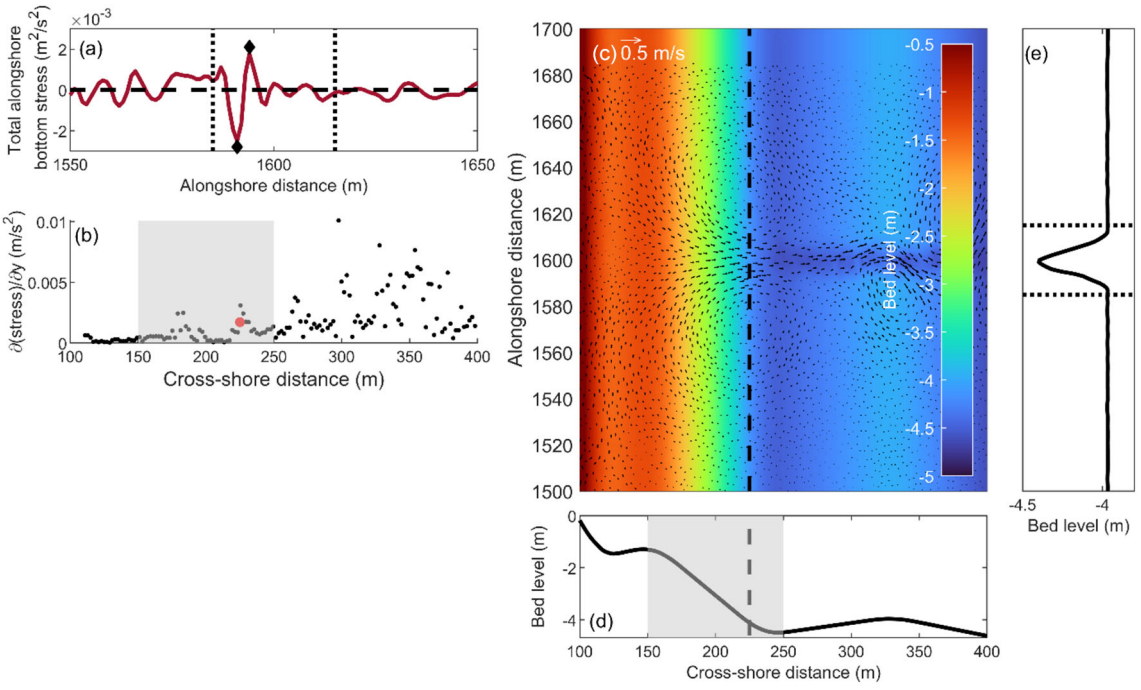

FIGURE 4 a) Total alongshore bottom stress (equation 1) versus alongshore distance at x = 225 m for a case 2 simulation (0.35 m deep and 30 m wide perturbation) hour 1. Positive values are stresses towards the south (left) and negative values are stresses towards the north (right). b) ∂stress/∂y versus cross-shore distance, and (c) flow pattern as a function of alongshore and cross-shore distance overlaid on colour contours of the bathymetry (scale on the right), and with the black dashed line indicating x = 225 m. d) Bed level versus cross-shore distance with vertical black dashed line at x = 225 m, and (e) bed level versus alongshore distance at x = 329 m with horizontal dotted black lines indicating the channel area. In (a), the black diamonds highlight the local maximum and minimum total alongshore stress contributions within the channel area (shown by vertical dotted lines) used to calculate the alongshore stress gradient shown in (b). In (b) and (d), the grey shaded area indicates the area from the outer-bar trough to inner-bar crest over which the ∂ stress/∂y is summed.

$$DSL = D * SL \quad (2)$$

That is used to identify cases resulting in inner-bar rip channel evolution.

3 | RESULTS

From among the twenty-three simulated cases with different initial bathymetries, four simulations for the Case 1 bathymetry and eleven for the Case 2 bathymetry resulted in the erosion of rip channels across the inner bar, indicating the presence of a persistent rip current. Consistent with prior results, the simulations suggest inner-bar rip generation depends on the cross-shore profile and the dimensions of the perturbation in the outer bar. Specifically, for the cases generating an inner-bar rip, DSL at the outer bar exceeded 0.0028 for Case 1 and 0.0016 for Case 2. The DSL-values were below these thresholds for seven of the eight cases that did not generate inner-bar rips (one Case 1 simulation with DSL = 0.0033 also did not erode a rip channel).

The DSL parameter is expected to be related to the amount of alongshore rip current forcing (Moulton et al., 2017; Winter et al., 2014). Hence, a relation between DSL (Equation 2) and alongshore stress (Equation 1) is examined. For the eight cases not eroding a rip channel, the sum of the alongshore stress gradients (∂(stress)/∂y) over the cross-shore distance from the outer-bar trough to the inner-bar crest (i.e., sum of data points within the grey shaded area in Figure 4b) is several factors smaller than for the remaining cases (not shown). This result suggests that the absence of an eroding inner-bar channel is due to weak rip currents. Moreover, simulated rip currents over the inner bar occurred only occasionally (predominantly during low tide) and were highly variable in their alongshore position (not shown).

For the 15 cases with rip generation over the inner bar, the sum of the alongshore stress gradients (∂(stress)/∂y) correlates linearly with outer-bar DSL (Figure 5a). For the 11 Case 2 simulations the squared correlation is 0.7 suggesting that the deeper and narrower the channel in the outer bar, the larger the stress gradient (and thus the feeder and rip current forcing) is at the inner bar, and thus, the maximum simulated rip current velocity at the inner-bar crest at hour 1 increases with increasing outer-bar DSL (Figure 5b, the squared correlation for the 11 Case 2 simulations is 0.8).

For the Case 1 bathymetries, the higher DSL threshold for inner-bar rip generation also implies that rip current velocities are lower compared with those on the Case 2 bathymetries for similar DSL (compare blue and red dots in Figure 5b). This result is likely related to the larger water depths over the bars. If Case 1 bed levels are increased by 1.2 m whereby the inner-bar depth becomes similar to the Case 2 bathymetry (z_{crest} = 1.3 m, Figure 2), the rip current velocities increase (compare blue dots with blue stars in Figure 5b) and follow the trend line of the Case 2 simulations (dotted red line). Not only do different bathymetries result in different DSL thresholds for triggering of rip channel formation, the wave conditions also matter. Simulations conducted for a subset of the bathymetry cases with stronger forcing conditions (H_s = 4 m, T_p = 10 s and *DSD* = 20°) show larger alongshore stress gradients and rip current velocities, but similar

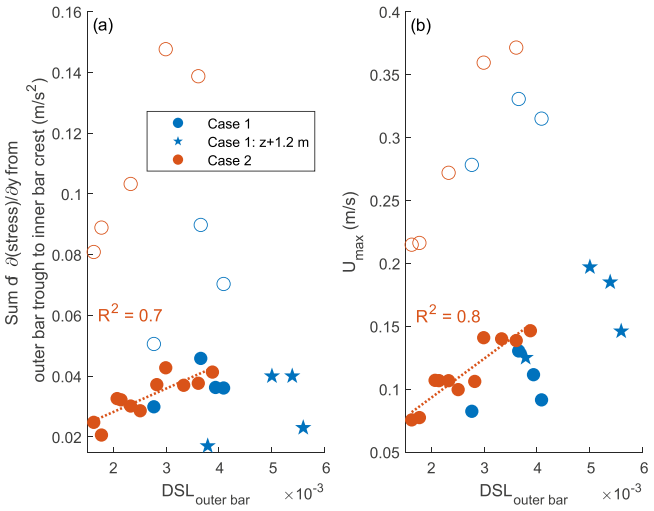

FIGURE 5 (a) The sum of alongshore stress gradients from the outer-bar trough to the inner-bar crest (hour 1), and (b) the maximum rip velocity over the inner-bar versus outer-bar DSL (hour 1) for Case 1 (blue) and Case 2 (red). The stars are Case 1 simulations with a + 1.2 m shift in the initial bathymetry. The open symbols are for the same bathymetries as Cases 1 and 2, but with wave conditions with H_s = 4 m, T_p = 10 s and DSD = 20°. The dotted red lines are the best linear fit to the Case 2 (red) simulations (squared correlation = 0.7 and 0.8, respectively).

trends of response (Figure 5). Hence, the DSL parameter appears to be important for rip channel generation. Additional hydrodynamic simulations conducted for the Case 2 bathymetry (initial DSL = 0.0018) for a range of wave conditions (Supporting Information Figure A) suggest that alongshore stress gradients and inner-bar rip current velocities increase with increasing H_s, T_p and with decreasing *DSD*.

During 5 days of simulated constant wave conditions, the inner-bar rip channel eroded and the rip current velocity increased (Figure 6, U_{max} is larger at hour 120 than at hour 1). Furthermore, larger initial U_{max} typically resulted in a larger velocity increase, suggesting that the outer-bar channel with the largest initial DSL (and thus the largest initial inner-bar rip current velocities) causes larger inner-bar channel erosion and even stronger inner-bar rips.

Not only the rip current velocity, but also the inner-bar channel position is correlated with the sum of the alongshore stress gradients (squared correlation R^2 = 0.6, Figure 7), suggesting the channel coupling depends on the perturbation geometry. Specifically, as the forcing of the alongshore feeder currents increases, the alongshore position of the inner-bar channel at hour 120 becomes closer to that of the outer-bar channel (y = 1,600 m), suggesting a tight coupling. Increased feeder convergence due to changing wave conditions also results in a tighter coupling between the outer and inner bar. For stronger wave forcing (open circles in Figure 7), the nearshore rip position was closer to y = 1,600 m than for the same initial outer bar channel but smaller waves (filled circles). In one case, however, the outer-bar channel accreted despite larger wave forcing and no nearshore rip was generated (the Case 1 bathymetry with the weakest initial alongshore stress gradient).

During the 5 days of simulation, rip current velocities fluctuated with the tide (strongest during low tide), but with an increasing trend as the inner-bar rip channel erodes (not shown). In cases of strong

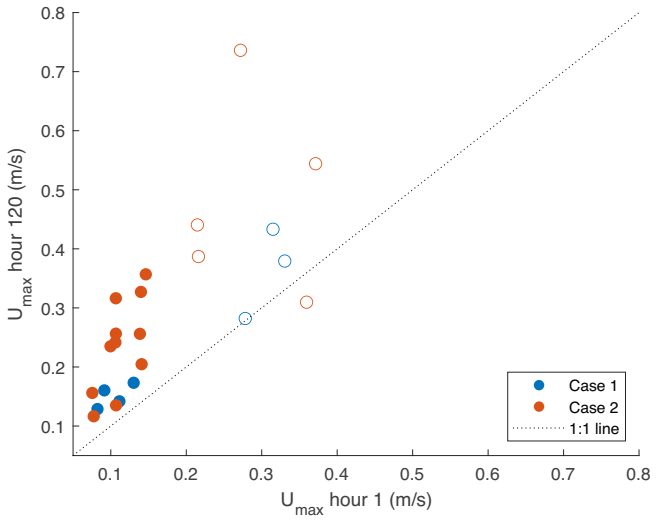

FIGURE 6 Maximum inner-bar rip current velocity during hour 120 versus that during hour 1 for Case 1 (blue) and Case 2 (red) bathymetries. The open symbols are for the same bathymetries as Cases 1 and 2, but with wave conditions with $H_s = 4$ m, $T_p = 10$ s and DSD = 20°.

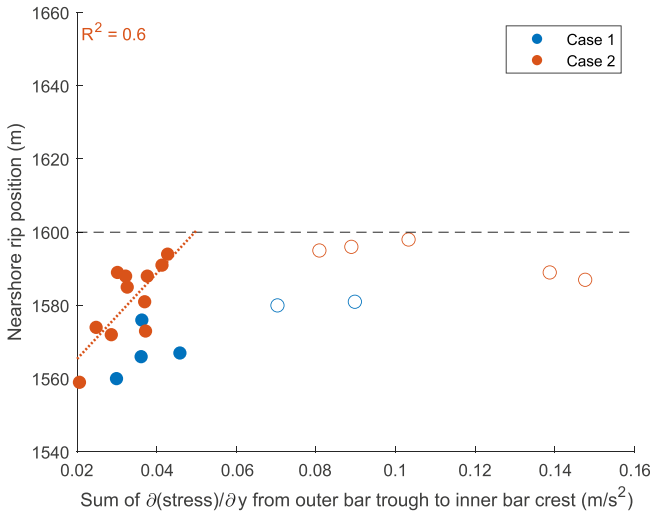

FIGURE 7 Alongshore position of the inner-bar rip channel at hour 120 versus the sum of initial alongshore stress gradients from the outer-bar trough to inner-bar crest for the Case 1 (blue) and Case 2 (red) bathymetry simulations. The dotted red line is the best linear fit ($R^2 = 0.6$) for the Case 2 simulations. The open symbols are for the same bathymetries as Cases 1 and 2, but with wave conditions with $H_s = 4$ m, $T_p = 10$ s and DSD = 20°. The horizontal dashed black line indicates the position of the channel in the outer bar.

forcing, the inner-bar rip channel grew at the same alongshore position throughout the modelling period. However, for weak forcing (resulting in weak stress gradients), the outer bar merely triggers the initiation of a rip channel in the area. For example, for the Case 2 bathymetry of initial DSL = 0.0018 that resulted in the weakest convergence (stress gradient = 0.02 m/s^2), the rip channel that eroded across the inner bar is located 40 m south of the channel in the outer bar (Figure 7). The time history of the bathymetry and flows (Figure 8) indicates that a weak rip current initially developed with

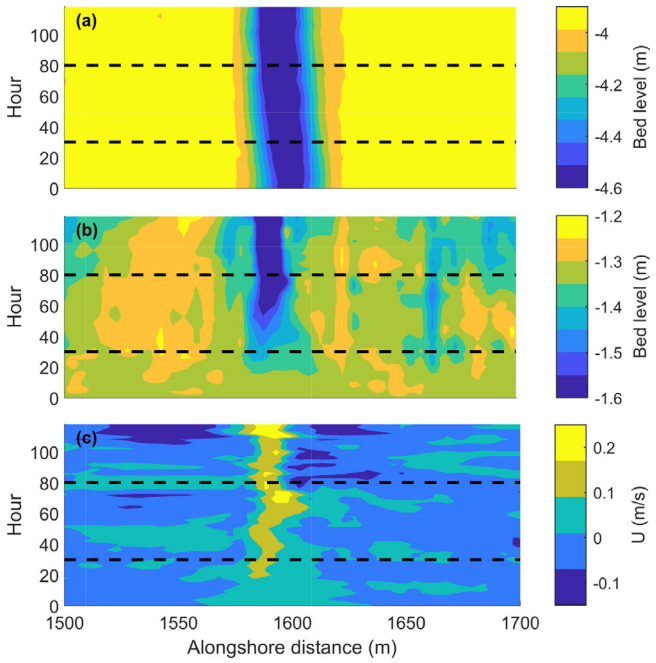

FIGURE 8 Color contours (scales on the right) as a function of time and alongshore distance of (a) bed level at x = 328 m, (b) bed level at x = 150 m and (c) cross-shore velocity (positive offshore) at x = 150 m for a Case 2 bathymetry with an initial perturbation in the outer bar of 0.41 m in the vertical and 49 m alongshore (DSL = 0.0018). Horizontal black dashed lines are drawn at hours 30 and 80.

offshore-directed flows near y = 1,600 m (Figure 8c, hours 5–10, turquoise). However, starting about hour 20, a stronger rip (> 0.1 m/s) was generated near y = 1,550 m with an eroding channel (Figure 8b), possibly indicating de-coupling between the two circulation patterns.

A simulation initialized with the bathymetry at hour 30, but with alongshore uniform bathymetry for x > 240 m, confirms that the inner-bar rip is not dependent on the outer-bar channel (Figure 9). Specifically, the cross-shore flow velocities at x = 150 m for the original simulation are similar to those from the simulation without the outer-bar channel (compare blue with green curve in Figure 9), with both simulations having an offshore-directed rip current between y = 1,520 and 1,580 m (positive velocities are offshore-directed).

However, the rip current is not stable near y = 1,550 m. From about hour 80 (Figure 8b), the inner-bar channel migrates towards y = 1,600 m and widens, resulting in decreasing rip flow velocities (Figure 8c). This evolution might be related to a re-established coupling between the inner and outer bar. At hour 80, the outer-bar DSL has increased to 0.0034 (from 0.0018 in hour 1) due to a deepening of the channel (Figure 8a), likely increasing the forcing from the outer bar (Figure 5a). A simulation initialized with the bathymetry at hour 80, but with alongshore uniform bathymetry for x < 240 m, generates an inner-bar rip channel at y = 1,578 m, suggesting that the increased DSL of the outer bar at hour 80 pushes the rip towards the north in the original simulation (Figure 8).

Summarizing the findings, inner-bar rip current velocity and alongshore channel location depend on the magnitude of the alongshore gradients of the feeder current bottom stresses, which are related to outer-bar DSL, H_s, T_p and *DSD*. For large forcings (resulting in strongly convergent feeder currents), rip current flows are fast and

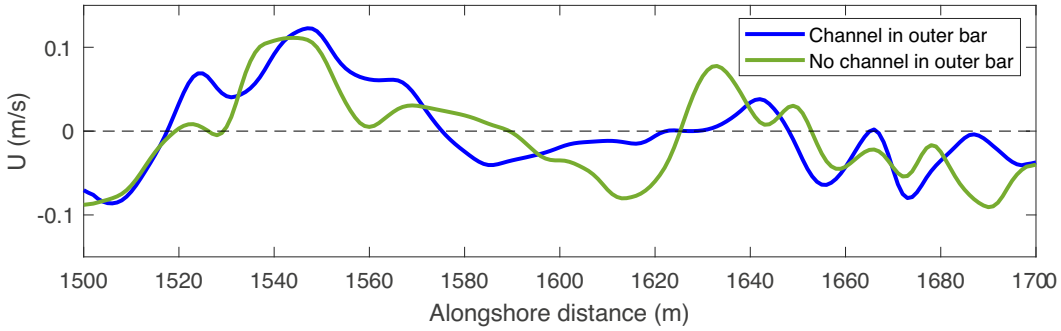

FIGURE 9 Cross-shore velocity at x = 150 m (the position of the inner-bar crest) versus alongshore distance at hour 30 for the original simulation with case 2 bathymetry and outer-bar DSL = 0.0018 (blue curve) and a simulation initialized with the hour 30 bathymetry, but without an outer-bar channel (green curve).

a strong spatial coupling exist between the outer- and inner-bar morphologies, with the erosion of a nearshore rip channel at the same alongshore position as the channel in the outer bar. In contrast, for weaker forcings, inner-bar rip current velocities decrease and the inner-channel location is less coupled to the outer bar, with the outer-bar channel triggering rip generation, but without maintaining it at the same alongshore position.

4 | DISCUSSION

The morphodynamic numerical simulations suggest that a single, medium scale (tens of centimeters in the vertical and tens of meters alongshore) perturbation in an outer bar can result in alongshore variable waves and flows at the inner bar, resulting in a rip current and channel erosion and coupling between the inner and outer sand bar. These findings are not inconsistent with previous studies of the coupling between bed perturbations and wave height patterns (bed-surf mechanisms) (Calvete et al., 2005; Falqués, Coco, & Huntley, 2000; Garnier et al., 2008), evolution of alongshore variability from initially straight bars (Nnafie et al., 2021; Thiébot et al., 2012), and inner-bar rip evolution with large-scale crescentic outer bars (Castelle et al., 2010a, 2010b). The minimum outer-bar channel dimensions that generated an inner-bar rip in this study were a depth of 0.41 m and width of 49 m (DSL = 0.0018), which is much smaller than in previous studies but twice the depth of the observed perturbation at Duck in 2013. This difference between observations and simulations does not exclude the possibility of outer-bar variability being responsible for the observed erosional hotspot generation. In particular, the field-calibrated MIKE21 model may underestimate the cross-shore flow velocities and the resulting channel evolution (Christensen, Raubenheimer, & Elgar, 2024b), possibly owing to the importance of 3-dimensional forcing that is neglected (Marchesiello et al., 2015). Rip velocities and channel widths and depths in single-barred systems increase with decreasing width and increasing depth of the initial bed perturbations (Brander, 1999; Calvete et al., 2007; Castelle et al., 2012; McCarroll et al., 2018). Similarly, here increasing the outer-bar channel depth and slope results in stronger nearshore current velocities and may compensate for the underprediction by the depth-averaged model. Thus, bar coupling might occur for even smaller DSL values than shown in the simulations here. Future studies using 3D models could potentially unravel the coupling processes further.

An overall DSL threshold for nearshore rip generation was not established for the wave conditions considered here. Specifically, for the Case 1 bathymetry, DSL values below 0.0028 did not result in nearshore rip channels, whereas for the Case 2 bathymetry, the DSL threshold was 0.0016. These different thresholds may be related to the different cross-shore positions and depths of the bars. For the Case 1 bathymetry, reduced bar depths resulted in increased rip current velocities, suggesting a decrease in DSL threshold (Figure 5b compare blue dots with stars). The outer bar depth is related to the cross-shore bar separation distance, which has been found to be important for inner-outer bar coupling and morphological evolution of double bar systems (Ruessink et al., 2007). Here, the cross-shore separation between the bars was roughly constant (about 180 m), but the alongshore forcing and resulting feeder bed stresses appear to decay with distance onshore of the outer bar (Figure 4b). Thus, consistent with prior studies (Ruessink et al., 2007), the coupling between the bars and flow patterns may increase (and the DSL thresholds may decrease) with decreasing separation distance (and decreasing depth of the outer bar).

The DSL thresholds for nearshore rip generation also depend on the wave conditions, with the sum of the alongshore stress gradients and the maximum rip current velocity increasing with wave height and period, whereas they decrease for increasing wave directional spreading (Figure A Supporting Information). This result suggests that for high-energy events of shore-normal and long-period waves, DSL thresholds will decrease compared with the cases studied here. Accordingly, free inner-bar rip channels (i.e., DSL value close to threshold) were not generated for any cases with $H_s = 4$ m, $T_p = 10$ s and $DSD = 20^\circ$ (Figure 7). Similarly, Price et al. (2013) showed the importance of wave direction for rip current development over the inner bar typically occurs only for close to shore-normal wave incidence (< 10°).

The spatial coupling between the outer- and inner-bar morphology depends on the outer-bar channel dimensions. For deep, narrow channels in the outer bar, the nearshore bathymetry mirrored the offshore bathymetry by eroding a channel at the same alongshore position as the outer-bar channel, consistent with the increasing importance of coupling found in prior studies with increasing perturbation height (Castelle et al., 2010b). Similar to a single-bar system, the stability of the rip location increases with perturbation height (Castelle et al., 2012). For a weak perturbation, a rip channel developed over the inner bar 40 m alongshore of the offshore channel position. Although random small-scale perturbations were not applied, it is possible that this alongshore-separated inner-bar rip channel arose from an instability and positive feedback mechanism (e.g., self-

organization). The generation of these free inner-bar rip channels is in keeping with general field observations that inner-bar rip channels are more irregularly spaced than the outer-bar channels. The findings that morphological coupling depends on the initial DSL as well as the wave forcing highlight the complexity of nearshore rip channel evolution and the feedback between the hydrodynamics and morphology.

5 | CONCLUSIONS

Simulations of a field-calibrated morphodynamic model (MIKE21) suggest that in double-barred systems, a single moderate-scale perturbation (O(0.1 m deep, 10 m wide)) in the outer-bar elevation can lead to the generation of a rip current and erosion of a rip channel across the inner bar. The model was driven with wave conditions and idealized bathymetry representative of field conditions during which strong rips and channel erosion were observed to occur over an inner bar. Consistent with prior results, the strength of the hydro-morphological coupling between the two bars depends on the dimensions of the outer-bar perturbation. The simulations suggest that for a given wave forcing, the magnitude of the inner-bar rip flow, the depth to which the inner-bar channel is eroded, and the alongshore position of the inner-bar rip relative to the outer-bar perturbation depend on the nondimensional outer-bar channel depth times the transverse rip-channel slope (DSL). The minimum threshold for inner-bar rip generation depends on both the DSL, the bar depths and the separation distance and the wave conditions. Systems with DSL near the minimum threshold may alternate between being coupled and uncoupled, with unstable locations of the inner-bar rip, whereas systems with large DSL tend to remain strongly coupled. Medium-scale perturbations in the outer bar can thus be important for the evolution of nearshore alongshore variability at a range of scales.

AUTHOR CONTRIBUTIONS

Drude Fritzbøger Christensen: funding acquisition; methodology; writing – initial draft; writing – reviewing and editing. **Britt Raubenheimer**: conceptualization; funding acquisition; methodology; investigation; writing – reviewing, and editing. **Steve Elgar**: conceptualization; funding acquisition; methodology; investigation; writing – reviewing and editing.

ACKNOWLEDGEMENTS

We thank DHI for the use of their MIKE21 software, and Aart Kroon for insightful comments on the manuscript. Funding was provided by the Villum Foundation, the US National Science Foundation and a Vannevar Bush Faculty Fellowship.

DATA AVAILABILITY STATEMENT

Model simulations were performed in the software package MIKE21 (version 2020), and the output files needed to evaluate or reproduce the results are available at 10.17894/ucph.c88dc824-6ae7-4e15-b110-2e71360a9525 (Christensen, Raubenheimer, & Elgar, 2024a).

ORCID

Drude Fritzbøger Christensen https://orcid.org/0000-0002-4271-981X

REFERENCES

Aagaard, T., Greenwood, B. & Nielsen, J. (1997) Mean currents and sediment transport in a rip channel. *Marine Geology*, 140(1–2), 25–45. Available from: https://doi.org/10.1016/S0025-3227(97)00025-X

Almar, R., Castelle, B., Ruessink, B.G., Sénéchal, N., Bonneton, P. & Marieu, V. (2010) Two- and three-dimensional double-sandbar system behaviour under intense wave forcing and a meso–macro tidal range. *Continental Shelf Research*, 30(7), 781–792. Available from: https://doi.org/10.1016/j.csr.2010.02.001

Anderson, D., Bak, A.S., Cohn, N., Brodie, K.L., Johnson, B. & Dickhudt, P. (2023) The impact of inherited morphology on sandbar migration during mild wave seasons. *Geophysical Research Letters*, 50(3), e2022GL101219. Available from: https://doi.org/10.1029/2022GL101219

Badru, G.S., Odunuga, S.S., Omojola, A.S. & Oladipo, E.O. (2022) Numerical modelling of sediment transport in southwest coast of Nigeria: implications for sustainable management of coastal erosion in the bight of Benin. *Journal of African Earth Sciences*, 187, 104466. Available from: https://doi.org/10.1016/j.jafrearsci.2022.104466

Birkemeier, W. A. (1985) Time scales of nearshore profile change. In *19th International Conference on Coastal Engineering* pp. 1507–1521 ASCE

Bowen, A.J. & Inman, D.L. (1969) Rip currents: 2. Laboratory and field observations. *Journal of Geophysical Research*, 74(23), 5479–5490. Available from: https://doi.org/10.1029/JC074i023p05479

Bowen, A.J. & Inman, D.L. (1971) Edge waves and crescentic bars. *Journal of Geophysical Research*, 76(36), 8662–8671. Available from: https://doi.org/10.1029/JC076i036p08662

Brander, R.W. (1999) Field observations on the morphodynamic evolution of a low-energy rip current system. *Marine Geology*, 157(3–4), 199–217. Available from: https://doi.org/10.1016/S0025-3227(98)00152-2

Brander, R.W. (2015) Rip Currents. In: *Coastal and marine hazards, risks, and disasters*. Amsterdam: Elsevier, pp. 335–379 https://doi.org/10.1016/B978-0-12-396483-0.00012-1

Cáceres, R.A., Zyserman, J.A. & Perillo, G.M.E. (2016) Analysis of sedimentation problems at the entrance to Mar del Plata harbor. *Journal of Coastal Research*, 32(2), 301. Available from: https://doi.org/10.2112/JCOASTRES-D-14-00056.1

Calvete, D., Coco, G., Falqués, A. & Dodd, N. (2007) (Un)predictability in rip channel systems. *Geophysical Research Letters*, 34(5), L05605. Available from: https://doi.org/10.1029/2006GL028162

Calvete, D., Dodd, N., Falqués, A. & van Leeuwen, S.M. (2005) Morphological development of rip channel systems: Normal and near-normal wave incidence. *Journal of Geophysical Research*, 110(C10), C10006. Available from: https://doi.org/10.1029/2004JC002803

Castelle, B., Marieu, V. & Bujan, S. (2019) Alongshore-variable beach and dune changes on the timescales from days (storms) to decades along the rip-dominated beaches of the Gironde coast, SW France. *Journal of Coastal Research*, 88(sp1), 157. Available from: https://doi.org/10.2112/SI88-012.1

Castelle, B., Marieu, V., Bujan, S., Splinter, K.D., Robinet, A., Sénéchal, N., et al. (2015) Impact of the winter 2013–2014 series of severe Western Europe storms on a double-barred sandy coast: beach and dune erosion and megacusp embayments. *Geomorphology*, 238, 135–148. Available from: https://doi.org/10.1016/j.geomorph.2015.03.006

Castelle, B., Marieu, V., Coco, G., Bonneton, P., Bruneau, N. & Ruessink, B.G. (2012) On the impact of an offshore bathymetric anomaly on surf zone rip channels. *Journal of Geophysical Research: Earth Surface*, 117(F1), F01038. Available from: https://doi.org/10.1029/2011JF002141

Castelle, B., Ruessink, B.G., Bonneton, P., Marieu, V., Bruneau, N. & Price, T.D. (2010a) Coupling mechanisms in double sandbar systems. Part 1: patterns and physical explanation. *Earth Surface Processes and Landforms*, 35, 476–486. Available from: https://doi.org/10.1002/esp.1929

Castelle, B., Ruessink, B.G., Bonneton, P., Marieu, V., Bruneau, N. & Price, T.D. (2010b) Coupling mechanisms in double sandbar systems. Part 2: impact on alongshore variability of inner-bar rip channels. *Earth Surface Processes and Landforms*, 35, 771–781. Available from: https://doi.org/10.1002/esp.1949

Christensen, D. F., Raubenheimer, B. & Elgar, S. (2024a) MIKE21 simulation outputs for double bar systems [dataset]. Electronic Research Data Archive. https://doi.org/10.17894/ucph.c88dc824-6ae7-4e15-b110-2e71360a9525

Christensen, D.F., Raubenheimer, B. & Elgar, S. (2024b) The roles of bathymetry and waves in rip-cshannel dynamics. *Journal of Geophysical Research: Earth Surface*, 129, e2023JF007389. Available from: https://doi.org/10.1029/2023JF007389

Coco, G., Calvete, D., Ribas, F., De Swart, H.E. & Falqués, A. (2020) Emerging crescentic patterns in modelled double sandbar systems under normally incident waves. *Earth Surface Dynamics*, 8(2), 323–334. Available from: https://doi.org/10.5194/esurf-8-323-2020

Dalrymple, R.A., MacMahan, J.H., Reniers, A.J.H.M. & Nelko, V. (2011) Rip currents. *Annual Review of Fluid Mechanics*, 43(1), 551–581. Available from: https://doi.org/10.1146/annurev-fluid-122109-160733

DHI. (2017a) MIKE 21—Spectral Wave Module—Scientific Documentation DHI Group

DHI. (2017b) MIKE 21 flow model & MIKE 21 flood screening tool—hydrodynamic module DHI Group

DHI. (2020) MIKE 21 & MIKE 3 flow model FM - Sand transport module—scientific documentation DHI Group

Dusek, G. & Seim, H. (2013) A probabilistic rip current forecast model. *Journal of Coastal Research*, 289, 909–925. Available from: https://doi.org/10.2112/JCOASTRES-D-12-00118.1

Elgar, S., Dooley, C., Gorrell, L. & Raubenheimer, B. (2023) Observations of two-dimensional turbulence in the surfzone. *Physics of Fluids*, 35(8), 085142. Available from: https://doi.org/10.1063/5.0159170

Engelund, F. & Fredsøe, J. (1976) A sediment transport model for straight alluvial channels. *Nordic Hydrology*, 7, 296–306.

Evans, O.F. (1940) The low and ball of the eastern shore of Lake Michigan. *The Journal of Geology*, 48(5), 476–511. Available from: https://doi.org/10.1086/624905

Falqués, A., Coco, G. & Huntley, D.A. (2000) A mechanism for the generation of wave-driven rhythmic patterns in the surf zone. *Journal of Geophysical Research: Oceans*, 105(C10), 24071–24087. Available from: https://doi.org/10.1029/2000JC900100

Fredsøe, J., Andersen, O.H. & Silberg, S. (1985) Distribution of suspended sediment in large waves. *Journal of Waterway, Port, Coastal, and Ocean Engineering*, 3(6), 1041–1059.

Gallagher, E.L., Elgar, S. & Guza, R.T. (1998) Observations of sand bar evolution on a natural beach. *Journal of Geophysical Research: Oceans*, 103(C2), 3203–3215. Available from: https://doi.org/10.1029/97JC02765

Garnier, R., Calvete, D., Falqués, A. & Dodd, N. (2008) Modelling the formation and the long-term behavior of rip channel systems from the deformation of a longshore bar. *Journal of Geophysical Research*, 113(C7), C07053. Available from: https://doi.org/10.1029/2007JC004632

Haller, M.C., Dalrymple, R.A. & Svendsen, I.A. (2002) Experimental study of nearshore dynamics on a barred beach with rip channels. *Journal of Geophysical Research*, 107(C6), 3061. Available from: https://doi.org/10.1029/2001JC000955

Hoefel, F. & Elgar, S. (2003) Wave-induced sediment transport and sandbar migration. *Science*, 299(5614), 1885–1887. Available from: https://doi.org/10.1126/science.1081448

Houser, C., Wernette, P., Trimble, S. & Locknick, S. (2020) Rip currents. In: *Sandy Beach Morphodynamics*. Amsterdam: Elsevier, pp. 255–276 https://doi.org/10.1016/B978-0-08-102927-5.00011-4

Isobe, M. & Horikawa, K. (1982) Study on water particle velocities of shoaling and breaking waves. *Coastal Engineering*, 25(1), 109–123. Available from: https://doi.org/10.1080/05785634.1982.11924340

Klein, M.D. & Schuttelaars, H.M. (2006) Morphodynamic evolution of double-barred beaches. *Journal of Geophysical Research*, 111(C6), C06017. Available from: https://doi.org/10.1029/2005JC003155

Kumar, N., Voulgaris, G. & Warner, J.C. (2011) Implementation and modification of a three-dimensional radiation stress formulation for surf zone and rip-current applications. *Coastal Engineering*, 58(12), 1097–1117. Available from: https://doi.org/10.1016/j.coastaleng.2011.06.009

Lippmann, T.C., Holman, R.A. & Hathaway, K.K. (1993) Episodic, nonstationary behavior of a double bar system at duck, North Carolina, U.S.a., 1986–1991. *Journal of Coastal Research*, 15, 49–75.

Loureiro, C., Ferreira, Ó. & Cooper, J.A.G. (2012) Extreme erosion on high-energy embayed beaches: influence of megarips and storm grouping. *Geomorphology*, 139–140, 155–171. Available from: https://doi.org/10.1016/j.geomorph.2011.10.013

Marchesiello, P., Benshila, R., Almar, R., Uchiyama, Y., McWilliams, J.C. & Shchepetkin, A. (2015) On tridimensional rip current modeling. *Ocean Modelling*, 96, 36–48. Available from: https://doi.org/10.1016/j.ocemod.2015.07.003

McCarroll, R.J., Brander, R.W., Scott, T. & Castelle, B. (2018) Bathymetric controls on rotational surfzone currents. *Journal of Geophysical Research: Earth Surface*, 123(6), 1295–1316. Available from: https://doi.org/10.1029/2017JF004491

Moulton, M., Elgar, S., Raubenheimer, B., Warner, J.C. & Kumar, N. (2017) Rip currents and alongshore flows in single channels dredged in the surf zone. *Journal of Geophysical Research: Oceans*, 122(5), 3799–3816. Available from: https://doi.org/10.1002/2016JC012222

Nnafie, A., Driessen, A.S., De Swart, H.E. & Price, T.D. (2021) Modelling the response of a double-barred sandy beach system to time-varying wave angles. *Earth Surface Processes and Landforms*, 46(7), 1393–1409. Available from: https://doi.org/10.1002/esp.5107

Petropoulos, A., Kapsimalis, V., Evelpidou, N., Karkani, A. & Giannikopoulou, K. (2022) Simulation of the nearshore sediment transport pattern and beach morphodynamics in the semi-Enclosed Bay of Myrtos, Cephalonia Island, Ionian Sea. *Journal of Marine Science and Engineering*, 10(8), 1015. Available from: https://doi.org/10.3390/jmse10081015

Price, T.D., Castelle, B., Ranasinghe, R. & Ruessink, B.G. (2013) Coupled sandbar patterns and obliquely incident waves. *Journal of Geophysical Research: Earth Surface*, 118(3), 1677–1692. Available from: https://doi.org/10.1002/jgrf.20103

Price, T.D. & Ruessink, B.G. (2011) State dynamics of a double sandbar system. *Continental Shelf Research*, 31(6), 659–674. Available from: https://doi.org/10.1016/j.csr.2010.12.018

Quartel, S. (2009) Temporal and spatial behaviour of rip channels in a multiple-barred coastal system. *Earth Surface Processes and Landforms*, 34(2), 163–176. Available from: https://doi.org/10.1002/esp.1685

Ruessink, B.G., Coco, G., Ranasinghe, R. & Turner, I.L. (2007) Coupled and noncoupled behavior of three-dimensional morphological patterns in a double sandbar system. *Journal of Geophysical Research*, 112(C7), C07002. Available from: https://doi.org/10.1029/2006JC003799

Ruessink, B.G., Pape, L. & Turner, I.L. (2009) Daily to interannual cross-shore sandbar migration: observations from a multiple sandbar system. *Continental Shelf Research*, 29(14), 1663–1677. Available from: https://doi.org/10.1016/j.csr.2009.05.011

Ruessink, B.G., Van Enckevort, I.M.J., Kingston, K.S. & Davidson, M.A. (2000) Analysis of observed two- and three-dimensional nearshore bar behaviour. *Marine Geology*, 169(1–2), 161–183. Available from: https://doi.org/10.1016/S0025-3227(00)00060-8

Short, A.D. & Aagaard, T. (1993) Single and multi-bar beach change models. *Journal of Coastal Research*, 15, 141–157.

Smit, M.W.J., Reniers, A.J.H.M., Ruessink, B.G. & Roelvink, J.A. (2008) The morphological response of a nearshore double sandbar system to constant wave forcing. *Coastal Engineering*, 55(10), 761–770. Available from: https://doi.org/10.1016/j.coastaleng.2008.02.010

Splinter, K.D., Gonzalez, M.V.G., Oltman-Shay, J., Rutten, J. & Holman, R. (2018) Observations and modelling of shoreline and multiple sandbar behaviour on a high-energy meso-tidal beach. *Continental Shelf Research*, 159, 33–45. Available from: https://doi.org/10.1016/j.csr.2018.03.010

Thiébot, J., Idier, D., Garnier, R., Falqués, A. & Ruessink, B.G. (2012) The influence of wave direction on the morphological response of a double sandbar system. *Continental Shelf Research*, 32, 71–85. Available from: https://doi.org/10.1016/j.csr.2011.10.014

Thornton, E.B., MacMahan, J. & Sallenger, A.H. (2007) Rip currents, megacusps, and eroding dunes. *Marine Geology*, 240(1–4), 151–167. Available from: https://doi.org/10.1016/j.margeo.2007.02.018

Valipour, A. & Bidokhti, A.A. (2018) An analytical model for the prediction of rip spacing in intermediate beaches. *Journal of Earth System Science*, 127(8), 108. Available from: https://doi.org/10.1007/s12040-018-1013-5

Valipour, A., Khaniki, A.K. & Bidokhti, A.A. (2014) Investigating the reactions of rip current pattern and sediment transport in rip channel against changes of bed parameters using numerical simulations. *Indian Journal of Geo-Marine Sciences*, 43(5), 831–840.

Van Enckevort, I.M.J., Ruessink, B.G., Coco, G., Suzuki, K., Turner, I.L., Plant, N.G., et al. (2004) Observations of nearshore crescentic sandbars. *Journal of Geophysical Research*, 109(C6), C06028. Available from: https://doi.org/10.1029/2003JC002214

Winter, G., Van Dongeren, A.R., De Schipper, M.A. & Van Thiel De Vries, J.S.M. (2014) Rip currents under obliquely incident wind waves and tidal longshore currents. *Coastal Engineering*, 89, 106–119. Available from: https://doi.org/10.1016/j.coastaleng.2014.04.001

SUPPORTING INFORMATION

Additional supporting information can be found online in the Supporting Information section at the end of this article.

How to cite this article: Fritzbøger Christensen, D., Raubenheimer, B. & Elgar, S. (2025) The impact of outer-bar alongshore variability on inner-bar rip dynamics. *Earth Surface Processes and Landforms*, 50(6), e70086. Available from: https://doi.org/10.1002/esp.70086